Flow-pattern identification and nonlinear dynamics of gas-liquid two-phase flow in complex networks

Zhongke Gao and Ningde Jin*

School of Electrical Engineering and Automation, Tianjin University, Tianjin 300072, People's Republic of China

(Received 22 November 2008; revised manuscript received 11 May 2009; published 4 June 2009)

The identification of flow pattern is a basic and important issue in multiphase systems. Because of the complexity of phase interaction in gas-liquid two-phase flow, it is difficult to discern its flow pattern objectively. In this paper, we make a systematic study on the vertical upward gas-liquid two-phase flow using complex network. Three unique network construction methods are proposed to build three types of networks, i.e., flow pattern complex network (FPCN), fluid dynamic complex network (FDCN), and fluid structure complex network (FSCN). Through detecting the community structure of FPCN by the community-detection algorithm based on *K*-mean clustering, useful and interesting results are found which can be used for identifying five vertical upward gas-liquid two-phase flow patterns. To investigate the dynamic characteristics of gas-liquid two-phase flow, we construct 50 FDCNs under different flow conditions, and find that the power-law exponent and the network information entropy, which are sensitive to the flow pattern transition, can both characterize the nonlinear dynamics of gas-liquid two-phase flow. Furthermore, we construct FSCN and demonstrate how network statistic can be used to reveal the fluid structure of gas-liquid two-phase flow. In this paper, from a different perspective, we not only introduce complex network theory to the study of gas-liquid two-phase flow but also indicate that complex network may be a powerful tool for exploring nonlinear time series in practice.

DOI: 10.1103/PhysRevE.79.066303 PACS number(s): 47.55.Ca, 89.75.Fb, 05.45.Tp, 89.75.Da

I. INTRODUCTION

Gas-liquid two-phase flow very often exists in industrial applications such as filtration, lubrication, spray processes, natural gas networks, and nuclear reactor cooling. In the study of two-phase flow, flow patterns indicate how the phases are distributed and mixed due to the physical nature of the system. Two-phase flow patterns depend on the type of fluid-fluid combination, the flow rates and direction, and the conduit shape, size, and inclination. Further, heat and mass transfer rates, momentum loss, rate of back mixing, and pipe vibration all vary greatly with the flow patterns. Hence, it is quite important and necessary to discern the flow patterns and study the nonlinear dynamics in different flow patterns.

The early studies were mostly based on direct observations. High-speed photography technique, x-ray attenuation picture, and suchlike are some of the methods in which the flow patterns are detected from direct observations. Although these methods are inexpensive and, in most cases, easy to perform, they are to a great extent subjective. Moreover the major difficulty in direct observation, even using high-speed photography, is that the picture is often confusing and difficult to interpret, especially when dealing with high velocity flows. Furthermore, in order to increase the objectivity, indirect methods were developed. Such methods mainly deal with the fluctuating properties of two-phase flow, and the fluctuations can be observed in the local pressure, the instantaneous two-phase mixture ratio, and suchlike. Rouhani and Sohal [1], and Das and Pattanayak [2] pointed out that there is a correlation between flow patterns and the fluctuation characteristics of the two-phase flow properties. Hence, attempts at the characterization of gas-liquid two-phase flow patterns based on a combination of subjective judgments and objective methods have been made. Hubbard and Dukler [3] calculated the power spectral density (PSD) for two-phase pressure-drop signals. Jones and Zuber [4] and Vince and Lahey [5] employed transient x-ray attenuation techniques, and calculated the PSD and the probability density function for chordal void fraction fluctuations. Zhang *et al.* [6] calculated Shannon entropy of two-phase flow systems from the power spectral density. Daw and co-workers [7–9] interpreted experimental pressure-drop measurements from a complex gas-solid flow system in terms of the methods for chaotic time-series analysis, and discussed issues concerning the reconstruction of attractors from experimental chaotic time-series data using Taken's method of delays.

In recent years, with the development of modern signal processing techniques, there has been much progress in the software measurement techniques. Mi *et al.* [10] applied a neural network to two-phase flow pattern identification in a vertical channel using signals from electrical capacitance probes. Warsito and Fan [11] utilized a neural network-based multicriterion optimization image reconstruction technique for imaging multiphase flow systems from electrical capacitance tomography. Yan *et al.* [12] identified the two-component flow regimes using back-propagation networks. Xiao *et al.* [13] established the general description method of chaotic attractor morphological characteristic using referenced sections, and put forward a new gas-liquid two-phase flow pattern classification method by combining the chaotic attractor morphological feature parameters of different dimensions. Although there has been some achievement in the study of gas-liquid two-phase flow, in conditions close to a transition between two patterns, detecting the flow pattern is crucially difficult. Furthermore, due to the complex nature of

*Corresponding author; ndjin@tju.edu.cn

gas-liquid two-phase flow, theoretical analyses have not been able to describe this complex system perfectly.

Meanwhile, the past few years have witnessed dramatic advances in the field of complex networks since the publication of the seminal works of Watts and Strogatz [14] as well as Barabási and Albert [15]. Complex networks, which have been observed to arise naturally in a vast range of physical phenomena, can describe any complex system that contains massive units (or subsystems) with nodes representing the component units and edges standing for the interactions between them. Many complex systems have been examined from the viewpoint of complex networks. Examples include world wide web [16], metabolic networks [17], protein networks in the cell [18], traffic networks [19], sexual networks [20], earthquake networks [21], and human electroencephalogram networks [22]. These empirical studies have inspired researchers to develop a variety of techniques and models to help us understand or predict the behavior of complex systems [23–25]. Complex networks, which provide us with a new viewpoint and an effective tool for understanding a complex system from the relations between the elements in a global way, not only may be a powerful tool for revealing information embedded in time series [26–29] but also can be used for studying nonlinear dynamic systems that cannot be perfectly described by theoretical model.

In this paper, we apply complex networks to study gas-liquid two-phase flow. Three different network construction methods are proposed to build three types of networks, i.e., flow pattern complex network (FPCN), fluid dynamic complex network (FDCN), and fluid structure complex network (FSCN). We first construct the FPCN that contains 90 nodes using a unique method based on time-delay embedding and modularity, and identify five vertical upward gas-liquid two-phase flow patterns by detecting the community structure of the resulting network. Then, in order to study the nonlinear dynamics of gas-liquid two-phase flow, we construct 50 FDCNs under different flow conditions with each containing 2000 nodes. Moreover, we discuss the physical implications of network degree distribution using the method of chaotic recurrence plot. Based on the investigation on the relevant statistical characteristics of the 50 resulting networks and two complexity measures (Lempel and Ziv complexity and approximate entropy), we find that the power-law exponent and network information entropy, which are sensitive to the flow pattern transition, can both characterize the nonlinear dynamics of gas-liquid two-phase flow. Finally, after proposing a general method for constructing complex network based on phase-space reconstruction, we construct FSCN and demonstrate how network statistic can be used to reveal the fluid structure of gas-liquid two-phase flow. Applying complex networks to analyze the characteristics of gas-liquid two-phase flow measurement fluctuant signals could be useful exploration for revealing and understanding the flow pattern transmission mechanism which cannot be described accurately by mathematical model because of the complexity and uncertainty it owns.

II. DEFINITION OF FLOW PATTERNS

The vertical upward gas-liquid two-phase flow patterns in a pipe of inner diameter of 125 mm can be categorized into five classes on the basis of the visual and video observations and still photography, as well as the time-spatial characteristic map of interfaces. According to Hewitt [30], the five flow patterns, observed in our experiment, can be defined as follows (Fig. 1):

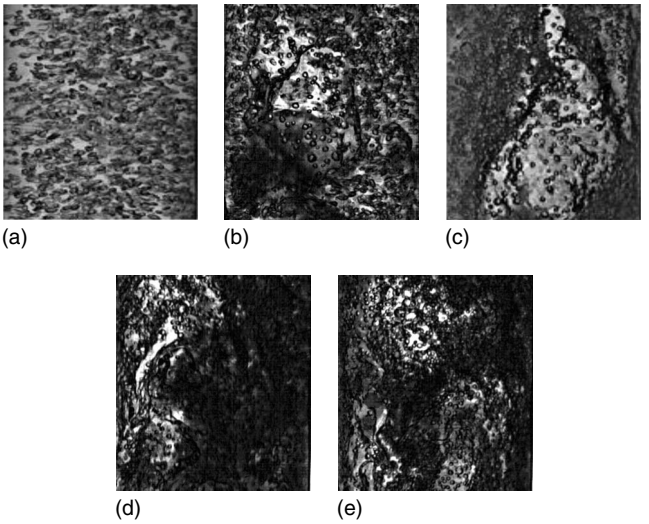

FIG. 1. The five vertical upward gas-liquid two-phase flow patterns recorded by high-speed VCR system. (a) Bubble flow; (b) bubble-slug transitional flow; (c) slug flow; (d) slug-churn transitional flow; (e) churn flow.

Bubble flow [Fig. 1(a)]: this flow pattern occurs at low gas flow rates where the gas phase is approximately uniformly distributed in the form of discrete bubbles in a continuum of liquid phase.

Bubble-slug transitional flow [Fig. 1(b)]: this flow pattern is characterized by the nonuniform distribution of the concentration of small bubbles in the flow direction. Small bubble coalescence occasionally occurs in the part of high bubble concentration, and as a result, a spherically capped bubble is formed.

Slug flow [Fig. 1(c)]: in this case, most of the gas appears in large bullet shaped bubbles, also known as Taylor bubbles, which have a diameter almost equal to the pipe diameter. The liquid slug area between two Taylor bubbles is filled with small bubbles that are very similar to those in bubble flow.

Slug-churn transitional flow [Fig. 1(d)]: with an increase in gas flow rate, for example, the gas-liquid interface of the larger gas bubble becomes distorted near the nose but still comparatively smooth in the bottom part of a cylindrical gas bubble.

Churn flow [Fig. 1(e)]: churn flow is a highly disordered flow that happens at high gas flow rates because of instabilities in the slugs. Churn flow can be interpreted as an irregular, chaotic, and disordered slug flow. It is also characterized by an oscillatory flow, with the liquid phase moving alternately upward and downward in the channel.

III. EXPERIMENTAL FLOW LOOP FACILITY AND DATA ACQUISITION

The gas-liquid two-phase flow experiment in a 125-mm-diameter vertical upward pipe was carried out in the multi-

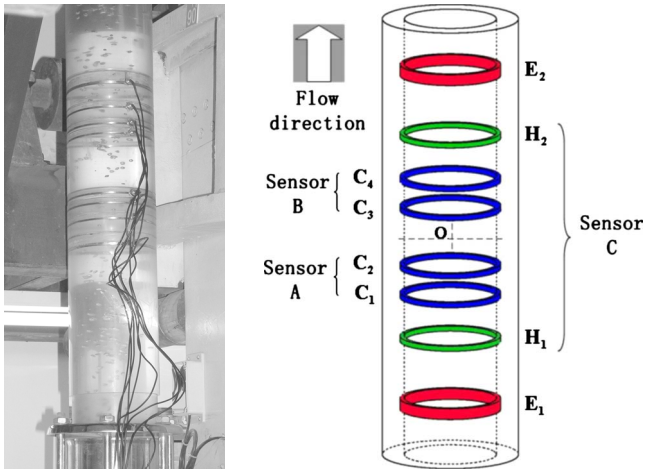

FIG. 2. (Color online) The vertical multielectrode array (VMEA) conductance sensor. (a) The VMEA measurement section; (b) the geometry of VMEA.

phase flow loop of Tianjin University. The whole measurement system can be divided into several parts, including the vertical multielectrode array (VMEA) conductance sensor that was designed and optimized by our research team [31], high-speed video camera recorder (VCR), exciting signals generating circuit, signal modulating module, data-acquisition device, and signal analysis software. The VMEA, as shown in Fig. 2, consists of eight alloy titanium ring electrodes axially separated and flush mounted on the inside wall of the flowing pipe. E_1 and E_2 are exciting electrodes. C_1-C_2 and C_3-C_4 are two pairs of upstream and downstream correlation electrodes denoted as sensors A and B, respectively. Based on the cross-correlation technique, we can extract the axial velocity of two-phase flow from fluctuating signals of sensors A and B. H_1-H_2 is the volume fraction electrodes denoted as sensor C. The fluctuating signals of sensor C are mainly correlated with the phase volume fraction. The measurement circuit is embedded inside the instrument, and signals were transmitted to the data acquisition and processing system through cable connected outside the circuit tube. The measurement system uses the 20 kHz constant voltage sine wave to excite, and the virtual value of exciting voltage is 1.4 V. The signal modulating module is mainly constituted of three modules, which are differential amplifier, sensitive demodulation, and low-pass filter. The data-acquisition equipment is selected from the National Instrument Co.'s product PXI 4472 data-acquisition card, which is based on the (PXI) PCI EXtensions for Instrumentation, a peripheral bus specialized for data acquisition and real-time control system main bus technology, equipped with eight channels and synchronized acquiring function. The data processing part is realized through graphical programming language LABVIEW 7.1 wrapped in the data-acquisition card, which can realize real time data waveform displaying, storing, and analyzing.

The experimental plan was such that first we put a fixed water flow rate into the pipe, then we gradually increased the gas flow rate; every time we finish the proportion of gas flow and water flow rates, we acquire one conductance fluctuating signal from VMEA, and observed the flow pattern variation by high-speed VCR. In the experiment, we set the resolution at 640×480, the frame rate at 200 frames per second. Figure 1 shows the five flow patterns of gas-liquid two-phase flow in a vertical upward pipe recorded by our high-speed VCR system. The water phase flow rate was between 1–14 m^3/h, of which the gas phase was between 0.2–130 m^3/h, and there are 90 different proportions of gas flow and water flow rates in this experiment. The sampling frequency was 400 Hz, and the sampling data recording time for one measuring point was 60 s. We have acquired 90 conductance fluctuating signals in the experiment all together. The conductance fluctuating signals in five flow patterns, measured from sensor C, are shown in Fig. 3, in which Q_g and Q_w represent gas flow and water flow rates, respectively.

Because of the significant difference in electrical sensibility between gas and liquid phases, the random flow of gas phase will cause voltage fluctuation on the measuring electrode under a certain sinusoidal input, which implies that the conductance fluctuating signals measured from the VMEA conductance sensor are related to the flow pattern transition. Thus, we construct complex networks from the conductance fluctuating signals and study the gas-liquid two-phase flow through analyzing the resulting networks.

IV. FLOW-PATTERN COMPLEX NETWORK

FPCN, extracted from the conductance fluctuating signals, is an abstract network, in which each flow condition is represented by a single node and the edge is determined by the strength of correlation between nodes. Flow condition here means the flow behavior under different proportion of gas flow and water flow rates in the pipe. Since we configured 90 different proportions of gas flow and water flow rates to get 90 conductance fluctuating signals in our gas-liquid two-phase flow experiment, there are 90 different flow conditions (i.e., the number of nodes contained in FPCN is 90), and each node corresponds to one of these 90 conductance fluctuating signals.

Note that the correlation between two nodes means the correlation between two corresponding conductance fluctuating signals. We now demonstrate how the strength of correlation between conductance fluctuating signals can be used to determine the edge. Considering the nonlinear characteristics of the gas-liquid two-phase flow, we first apply the method of time-delay embedding [32] to process the conductance fluctuating signals. That is, we use C-C method [33] to calculate the delay time τ from 90 conductance fluctuating signals, respectively, and choose the proper τ that can make the FPCN modularity [34] largest. Then we extract six time-domain features and four frequency-domain features from each processed conductance fluctuating signal to form the characteristic vector (see the following Sec. IV A for details). That is, there are 90 characteristic vectors and each vector contains ten elements. For each pair of characteristic vectors, $\mathbf{T_i}$ and $\mathbf{T_j}$, the correlation coefficient can be written as

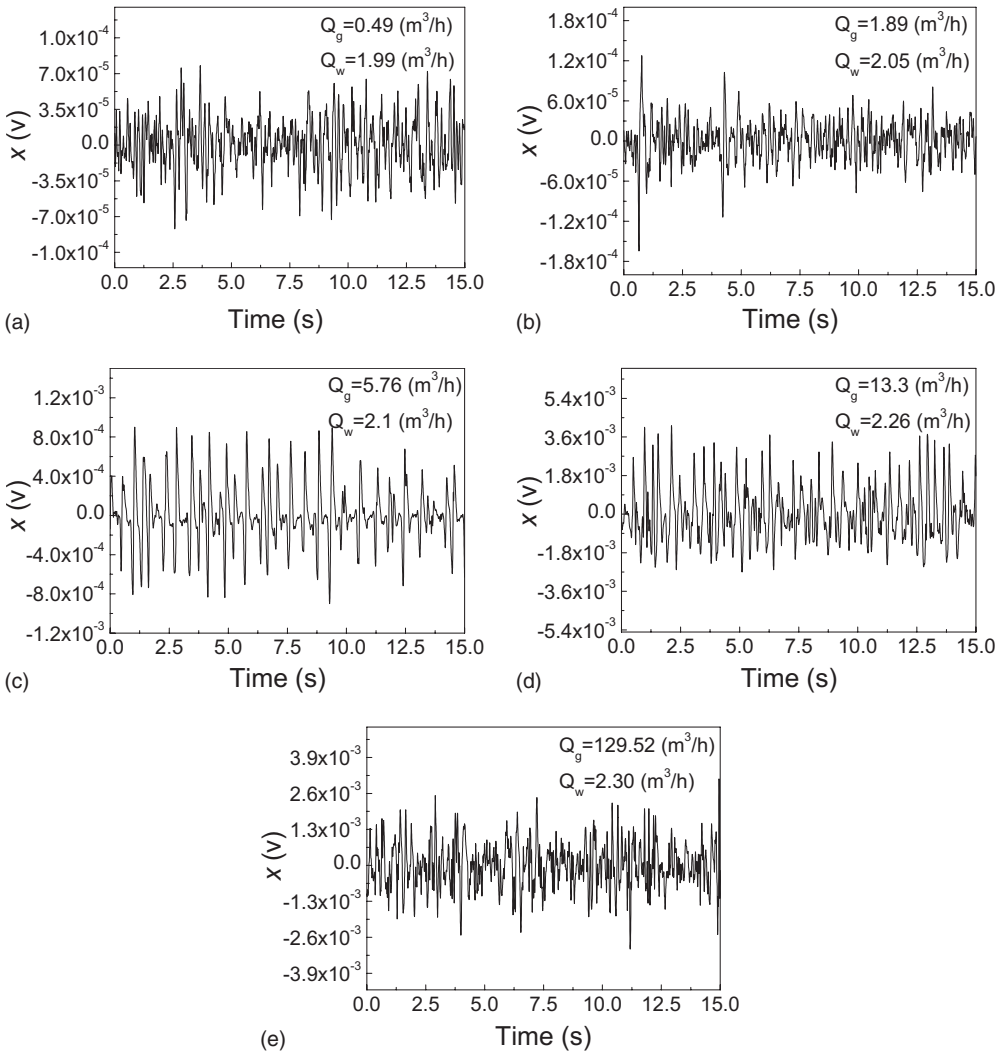

FIG. 3. The conductance fluctuating signals in five flow patterns. (a) Bubble flow; (b) bubble-slug transitional flow; (c) slug flow; (d) slug-churn transitional flow; (e) churn flow.

$$C_{ij} = \frac{\sum_{k=1}^{M} [\mathbf{T_i}(k) - \langle \mathbf{T_i} \rangle] \cdot [\mathbf{T_j}(k) - \langle \mathbf{T_j} \rangle]}{\sqrt{\sum_{k=1}^{M} [\mathbf{T_i}(k) - \langle \mathbf{T_i} \rangle]^2} \cdot \sqrt{\sum_{k=1}^{M} [\mathbf{T_j}(k) - \langle \mathbf{T_j} \rangle]^2}}, \quad (1)$$

where M is the dimension of the characteristic vector and $\langle \mathbf{T_i} \rangle = \sum_{k=1}^{M} \mathbf{T_i}(k)/M$, $\langle \mathbf{T_j} \rangle = \sum_{k=1}^{M} \mathbf{T_j}(k)/M$. The elements C_{ij} are restricted to the domain $-1 \le C_{ij} \le 1$, where $C_{ij}=1$, 0, and -1 correspond to perfect correlations, no correlations, and perfect anticorrelations, respectively. $\boldsymbol{C}$ is a symmetric matrix and C_{ij} describes the state of connection between nodes i and j. Finally, choosing a critical threshold r_c (see the following Sec. IV B for details), the correlation matrix $\boldsymbol{C}$ can be converted into adjacent matrix $\boldsymbol{A}$, the rules of which read:

$$\boldsymbol{A}_{ij} = \begin{cases} 1, & (|C_{ij}| \ge r_c) \\ 0, & (|C_{ij}| < r_c) \end{cases}. \quad (2)$$

That is, there will be an edge connecting nodes i and j if $|C_{ij}| \ge r_c$. On the other hand, there will not be an edge connecting nodes i and j if $|C_{ij}| < r_c$.

All the nodes and edges form the FPCN, and the topological structure of this network can be described with the adjacent matrix $\boldsymbol{A}$. The conditions $A_{ij}=1$ and $A_{ij}=0$ correspond to connection and disconnection, respectively.

A. Feature extraction from conductance fluctuating signals

In this study, we extract ten different kinds of feature quantities in both time and frequency domains. In the time domain, we choose the maximum value, minimum value, average value, standard deviation, asymmetry coefficient, and kurtosis function as the features of signals; in the frequency domain, we select the four coefficients of the linear prediction model with four orders.

Maximum value:

$$\mathrm{Max} = \max(x_1, x_2, \ldots, x_n). \tag{3}$$

Minimum value:

$$\mathrm{Min} = \min(x_1, x_2, \ldots, x_n). \tag{4}$$

Mean value:

$$\bar{x} = \frac{1}{n-1}\sum_{i=1}^{n} x_i. \tag{5}$$

Standard deviation:

$$S = \left(\frac{\sum_{i=1}^{n} (x_i - \bar{x})^2}{n-1} \right)^{1/2}. \tag{6}$$

Dissymmetry coefficient:

$$D = \frac{\sum_{i=1}^{n} (x_i - \bar{x})^3}{(n-1)S^2}. \tag{7}$$

Kurtosis coefficient:

$$K = \left(\frac{\sum_{i=1}^{n} (x_i - \bar{x})^4}{(n-1)S^4} \right) - 3. \tag{8}$$

The method of feature extraction in the frequency domain was mainly referred to the way used by Darwich *et al.* [35] which was based on the concept of linear prediction in speech signal processing [36]. The basic principle of this method is that the value of a signal point at present could be estimated by the linear combination of several previous points; the coefficient of this linear combination could be acquired when the deviation between the true value and the estimated value is minimum. The coefficients and previous signals comprise a linear prediction model; the coefficients are called the orders of this model, which are also what we set as the frequency characteristic quantities. We assumed that the input Z_t could be expressed as follows:

$$Z_t = -\sum_{k=l}^{p} a_k Z_{t-k} + G\sum_{l=0}^{q} b_l U_{t-l} \quad (b_0 = 1), \tag{9}$$

where U_{t-l} are the unknown input signals, $a_k(1 \le k \le p)$, $b_l(1 \le l \le q)$, and G are all system parameters, of which G is the system gain, and $a_k(1 \le k \le p)$, the coefficients of the linear combination, are just what we want as frequency characteristic quantities. We choose the linear prediction model with four orders, which means we only need to figure out a_1, a_2, a_3, and a_4. The detailed computation process can be seen in [36].

B. Selection of the threshold

Before demonstrating how to select a critical threshold r_c, here we first introduce a quality function or "modularity" Q, proposed by Newman *et al.* [34]. Let e_{ij} be the fraction of edges in the network that connect nodes in community i to those in community j, and let $a_i = \Sigma_j e_{ij}$. Then

$$Q = \sum_i (e_{ii} - a_i^2) \tag{10}$$

is the fraction of edges that fall within communities, minus the expected value of the same quantity if edges fall at random without regard for the community structure. If a particular division gives no more within-community edges than would be expected by random chance, we will get $Q=0$. Values other than zero indicate deviations from randomness, and in practice values greater than about 0.3 appear to indicate significant community structure [34].

The threshold r_c determines the characteristics of the resulting network. If it is extremely small, the pairs of nodes with weak correlations are also connected. The physically meaningful correlations in time series will be submerged by these noises. Increasing the value of r_c, the number of connections among the points becomes smaller and smaller. More and more of the noises are filtered out. But up to now, there has not been a general method for selecting critical threshold. In this study, we can expect a neighborhood of r_c, in which the structure of the resulting network can keep stable. That is, a critical threshold r_c can be found just by simulating a special dynamical process of the complex network, i.e., decreasing the number of connections by increasing the value of r_c while keeping the modularity of resulting network almost unchanged. If there exists a neighborhood of a threshold, in which the modularity of the resulting network has been almost the same, we assert that such threshold r_c is just what we need in this paper.

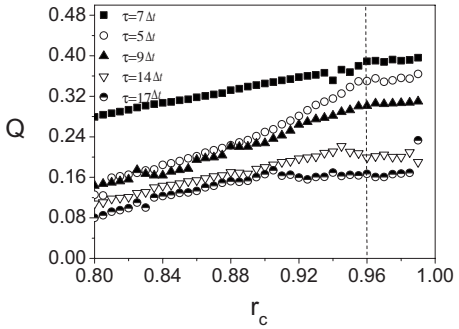

FIG. 4. The modularity distribution of FPCN with the change in delay time and threshold.

By calculation, the modularity distribution of FPCN with the change in delay time and threshold is shown in Fig. 4. As can be seen, the modularity Q keeps stable when r_c ranging from 0.965 to 0.985 and the modularity Q reaches the largest when $\tau = 7\Delta t$ (Δt is the sample interval of the conductance fluctuating signals). Therefore, according to the principle mentioned above, we choose $\tau = 7\Delta t$ and $r_c = 0.975$ to derive the FPCN.

V. FLOW-PATTERN IDENTIFICATION IN FPCN

A. Community-detection algorithm based on *K*-mean clustering

Community-detection algorithm based on K-mean clustering, proposed in this paper, means that we use K-mean ap-

proach to do clustering analysis on the data which are acquired through conversion by Capocci's approach [37] to reveal the network community structure.

Capocci approach: Capocci recasted the eigenproblem into an optimization problem. Let the standard matrix be defined as

$$\boldsymbol{N} = \boldsymbol{K}^{-1}\boldsymbol{A}. \tag{11}$$

Consider the following constrained optimization problem:

Let $z(x)$ be defined as

$$z(x) = \frac{1}{2}\sum_{i,j=1}^{n}(x_i - x_j)^2 A_{ij}, \tag{12}$$

where x_i are values assigned to the nodes, with some constraint on the vector $\boldsymbol{X}$, expressed by

$$\sum_{i,j=1}^{1} x_i x_j m_{ij} = 1, \tag{13}$$

where m_{ij} are elements of a given symmetric matrix $\boldsymbol{M}$. The stationary points of z over all $\boldsymbol{X}$ subject to constraint (12) are the solutions of

$$(\boldsymbol{D} - \boldsymbol{A})\boldsymbol{X} = \mu \boldsymbol{M}\boldsymbol{X}, \tag{14}$$

where $\boldsymbol{D}$ is the diagonal matrix:

$$\boldsymbol{D} = (d_{ij}) \tag{15}$$

$$d_{ij} = \delta_{ij}\sum_{k=1}^{n} A_{ik},$$

$\boldsymbol{A}$ is the adjacency matrix, n is the number of nodes, and μ is a Lagrange multiplier.

Different choices of the constraint $\boldsymbol{M}$ leads to different eigenvalue problems: for example, choosing $\boldsymbol{M}=\boldsymbol{D}$ leads to the eigenvalue problem $\boldsymbol{D}^{-1}\boldsymbol{A}\boldsymbol{X}=(1-2\mu)\boldsymbol{X}$, while $\boldsymbol{M}=\boldsymbol{I}$ leads to $(\boldsymbol{D}-\boldsymbol{A})\boldsymbol{X}=\mu\boldsymbol{X}$. Thus, $\boldsymbol{M}=\boldsymbol{D}$ and $\boldsymbol{M}=\boldsymbol{I}$ correspond to the eigenproblems for the (generalized) normal and Laplacian matrices, respectively.

Capocci *et al.* [37] have proven that, for a network with significant community structure, the first nontrivial eigenvector components of the standard matrix $\boldsymbol{N}$ could be used to study its community structure. Therefore, we use the eigenvectors of standard matrix to conduct the clustering analysis and then convert to the corresponding nodes to reveal the community structure.

B. Flow-pattern identification based on community structure

After constructing the FPCN containing 90 nodes, we show in Fig. 5 the distribution of the corresponding elements of the three first nontrivial eigenvectors. As can be seen, three different communities can be clearly identified when the components of the first nontrivial eigenvector a_1 are plotted versus those of a_2 and a_3. The community structure of the FPCN, detected by community-detection algorithm based on K-mean clustering, is shown in Fig. 6. The community structure is drawn by the software "UCINET" and "NETDRAW."

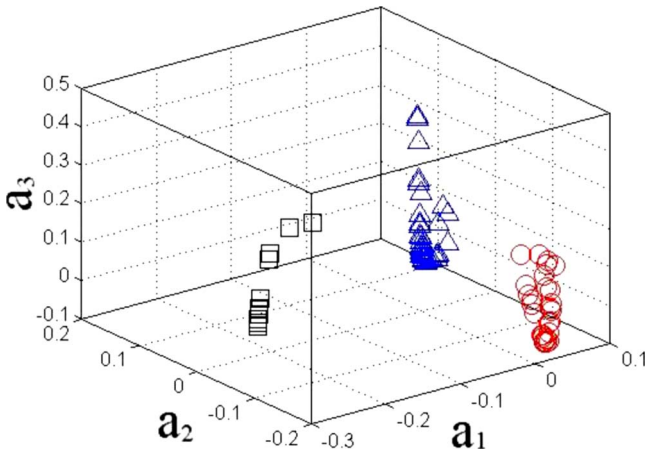

FIG. 5. (Color online) Components of the first nontrivial eigenvector a_1 are plotted versus those of a_2 and a_3.

From the detected community structure, as shown in Fig. 6, three communities of 21, 30, and 39 nodes are found, denoted as communities a, b, and c, respectively. Furthermore, combining with the experimental observations using high-speed VCR, we find that community a mainly corresponds to bubble flow, such as nodes 2 (Q_g=0.2 m^3/h, Q_w=2.0 m^3/h) and 16 (Q_g=0.94 m^3/h, Q_w=12.0 m^3/h) both corresponding to bubble flow; community b mainly corresponds to slug flow, such as nodes 31 (Q_g=2.1 m^3/h, Q_w=2.0 m^3/h) and 44 (Q_g=4.1 m^3/h, Q_w=6.0 m^3/h) both corresponding to slug flow; community c mainly corresponds to churn flow, such as nodes 70 (Q_g=69.0 m^3/h, Q_w=4.0 m^3/h) and 90 (Q_g=139.0 m^3/h, Q_w=2.0 m^3/h) both corresponding to churn flow; the nodes of the FPCN that connect tightly between communities a and b correspond to bubble-slug transitional flow, such as nodes 19 (Q_g=1.0 m^3/h, Q_w=2.0 m^3/h) and 26 (Q_g=1.7 m^3/h, Q_w=4.0 m^3/h) both corresponding to the bubble-slug transitional flow; the nodes of the FPCN that connect tightly between communities b and c correspond to slug-churn transitional flow, such as nodes 32 (Q_g=38.0 m^3/h, Q_w=8.0 m^3/h) and 58 (Q_g=25.0 m^3/h, Q_w=4.0 m^3/h) both corresponding to the slug-churn transitional flow. Hence, through detecting the community structure of the FPCN by the community-detection algorithm based on K-mean clustering, we have achieved good identification of gas-liquid two-phase flow pattern by finding the three communities which correspond to the bubble flow, slug flow, and churn

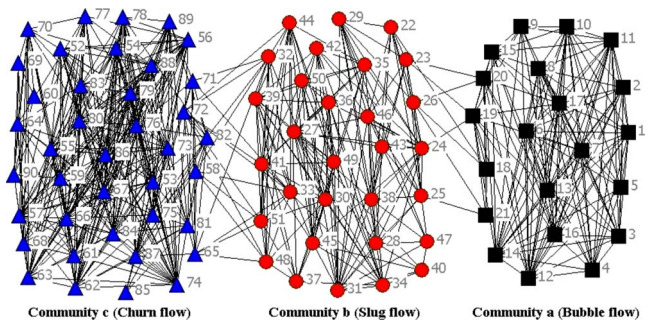

FIG. 6. (Color online) Community structure of the FPCN.

flow, respectively, and the nodes that connect tightly between two communities corresponding to the transitional flow.

VI. FLUID DYNAMIC COMPLEX NETWORK

To cast light into the nonlinear dynamics of gas-liquid two-phase flow, we construct FDCN from one conductance fluctuating signal with each segment of signal time series represented by a single node and edge determined by the strength of correlation between segments. Considering a conductance fluctuating signal (i.e., a time series), denoted as $\{k_1, k_2, k_3, \ldots\ldots, k_N\}$, we can obtain all the possible segments with length L, which read

$$\{\mathbf{S}_1 = (k_1, k_2, \ldots, k_L)\},$$

$$\{\mathbf{S}_2 = (k_2, k_3, \ldots, k_{L+1})\},$$

$$\{\mathbf{S}_3 = (k_3, k_4, \ldots, k_{L+2})\},$$

$$\vdots$$

$$\{\mathbf{S}_m = (k_m, k_{m+1}, k_{m+2}, \ldots, k_{m+L-1}) | m = 1, \ldots, N - L + 1\}. \tag{16}$$

For each pair of segments, $\mathbf{S_i}$ and $\mathbf{S_j}$, the correlation coefficient can be written as

$$C_{ij} = \frac{\sum_{k=1}^{L} [\mathbf{S_i}(k) \cdot \mathbf{S_j}(k)]}{\sqrt{\sum_{k=1}^{L} [\mathbf{S_i}(k)]^2} \cdot \sqrt{\sum_{k=1}^{L} [\mathbf{S_j}(k)]^2}}. \tag{17}$$

$\boldsymbol{C}$ is a symmetric matrix, and C_{ij} describes the state of connection between nodes i and j. Choosing a critical threshold r_c, the correlation matrix $\boldsymbol{C}$ can be converted into adjacent matrix $\boldsymbol{A}$, the rules of which read: $A_{ij}=1$ if $|C_{ij}| \geq r_c$ and $A_{ij}=0$ if $|C_{ij}| < r_c$.

Rho *et al.* [38] consider the characteristics of the degree distribution functions for the constructed networks. At a special critical threshold the degree distribution will tend to obey a power law. The network at this transition point is used to detect nontrivial characteristics embedded in the autocorrelation matrix. Through the analysis of the evolution of FDCN containing 2000 nodes, we find that the resulting network can keep well the physically meaningful correlations when r_c is chosen as 0.95 (see Fig. 7 for details).

The other adjustable parameter is the length of a segment, denoted as L. Short length will induce overestimated correlations [28]. Increasing the length L can depress the finite-length-induced statistical fluctuations effectively. It should be long enough to give a reliable result. As shown in Fig. 7, we find that, when r_c and L are chosen as 0.95 and 50, respectively, the degree distribution of the resulting network can be well fitted with a power law as follows:

$$p(k) \sim k^{-\gamma}, \tag{18}$$

where the degree (or connectivity) k of a node is the number of edges incident with it, and the degree distribution $p(k)$ is

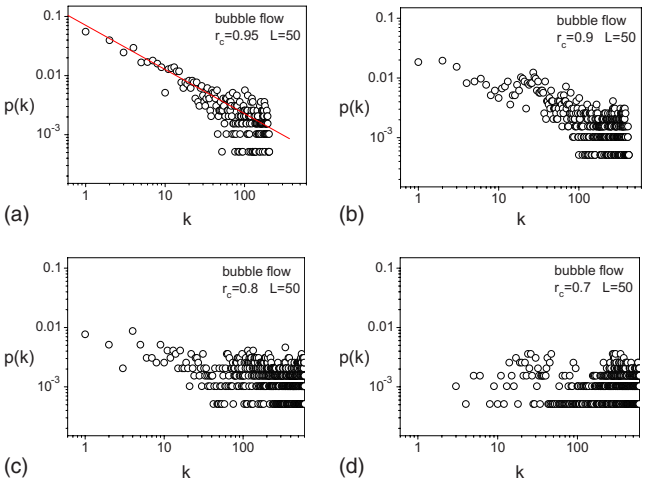

FIG. 7. (Color online) Evolution of the FDCN constructed from the conductance fluctuating signal of bubble flow (Q_g=0.2 m^3/h, Q_w=2.0 m^3/h). When r_c=0.95, the degree distribution obeys a power law. With the decrease in r_c, more and more edges are added, which may induce statistical fluctuations in the degree distribution. Finally, the power law is submerged in statistical noises. All the four figures are plotted in log-log scale.

defined as the probability that a node chosen uniformly at random has degree k; γ is the power-law exponent of degree distribution. In this study, we can expect a stability region of L, in which the resulting network can reveal the physically meaningful information embedded in the time series. That is, a proper L can be found just by simulating a special dynamical process of the complex network, i.e., changing the number of nodes and connections by increasing the value of L while keeping the power-law exponent of resulting network almost unchanged. By calculation, we plot the distribution of power-law exponent of different flow patterns in Fig. 8. From Fig. 8, it is clear that the power-law exponent keeps stable when L ranges from 45 to 55. Thus, we choose L =50 and r_c=0.95 to derive the FDCN.

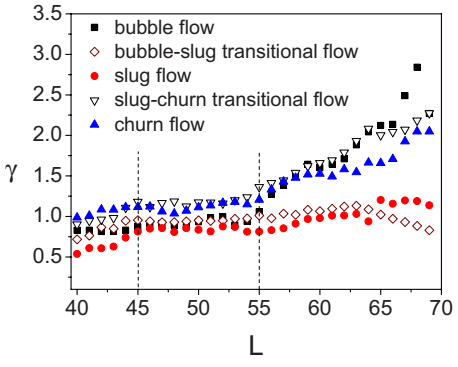

FIG. 8. (Color online) The power-law exponent distribution of five FDCNs with the change in segment length. Bubble flow (Q_g =0.2 m^3/h, Q_w=2.0 m^3/h); bubble-slug transitional flow (Q_g =1.0 m^3/h, Q_w=2.0 m^3/h); slug flow (Q_g=4.1 m^3/h, Q_w =6.0 m^3/h); slug-churn transitional flow (Q_g=25.0 m^3/h, Q_w =4.0 m^3/h); churn flow (Q_g=139.0 m^3/h, Q_w=2.0 m^3/h).

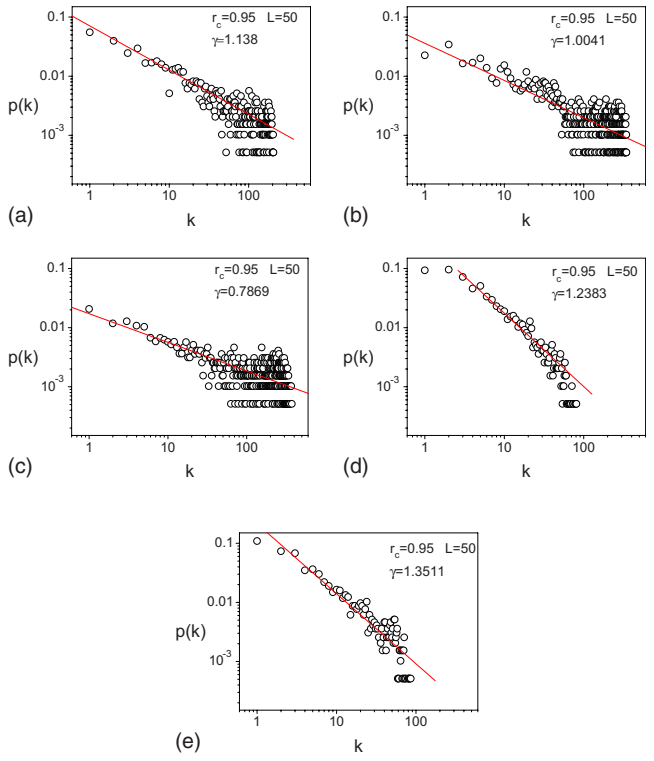

FIG. 9. (Color online) Degree distribution of different types of FDCNs in log-log scale. (a) Bubble flow (Q_g=0.2 m^3/h, Q_w =2.0 m^3/h); (b) bubble-slug transitional flow (Q_g=1.0 m^3/h, Q_w =2.0 m^3/h); (c) slug flow (Q_g=4.1 m^3/h, Q_w=6.0 m^3/h); (d) slug-churn transitional flow (Q_g=25.0 m^3/h, Q_w=4.0 m^3/h); (e) churn flow (Q_g=139.0 m^3/h, Q_w=2.0 m^3/h).

VII. FLUID DYNAMICS OF GAS-LIQUID TWO-PHASE FLOW IN FDCN

A. Network degree distribution and its physical implications

By considering segments as nodes and associating network connectivity with the correlation among segments, time-domain dynamics are naturally encoded into a network configuration. We select five types of flow pattern conductance fluctuating signals for constructing five FDCNs with each containing 2000 nodes. After investigating the degree distribution of the five networks, we find their degree distributions can be well fitted with a power law, which indicates the scale-free property of the FDCN (see Fig. 9 for details).

To reveal the physical implications of the degree distribution of FDCNs, the method of recurrence plot [39] is employed. The recurrence plots of the five typical conductance fluctuating signals are shown in Fig. 10. Because of the stochastic motion of large number of small bubbles, randomness is the main property of bubble flow conductance fluctuating signal, which can be reflected by the texture of its recurrence plot (i.e., large number of homogeneous discrete points) [see Fig. 10(a)]. But with the increase in gas superficial velocity due to the periodic alternating movement between gas and liquid plugs, the slug flow conductance fluctuating signal exhibits the periodic property to some extent, and this property can be reflected by the texture of slug flow recurrence plot (i.e., obvious linellaes along principal diagonal as well as the black intermittent rectangular blocks) [see Fig. 10(c)]. So the correlation of slug flow conductance fluctuating signal is much better than that of the bubble flow. Since the edges of FDCN are determined by the strength of correlation between segments of conductance fluctuating signal, there are more high degree nodes and less low degree nodes in the FDCN from slug flow than in the FDCN from bubble flow, just as shown in Figs. 9(a)–9(c). When the gas superficial velocity is high because of the unstable oscillation, the churn flow conductance fluctuating signal exhibits weak periodic property as well as random property, which can be reflected by the texture of churn flow recurrence plot (i.e., small black intermittent rectangular blocks as well as large number of homogeneous discrete points) [see Fig. 10(e)]. So there are less high degree nodes and more low degree nodes in the FDCN from churn flow than in the FDCN from slug flow, just as shown in Figs. 9(d) and 9(e).

More high degree nodes and less low degree nodes implies small degree distribution power-law exponent. In contrast, more low degree nodes and less high degree nodes implies large degree distribution power-law exponent. To further explore the variations in the degree distribution power-law exponent in flow pattern transition, we construct 50 FDCNs under different flow conditions and calculate their corresponding power-law exponents. From Fig. 11, we could see that the power-law exponents of bubble flow and bubble-slug transitional flow are usually large, and the power-law exponent decreases as the flow pattern evolves from bubble flow to slug flow. But with further increase in gas superficial velocity, the power-law exponent increases as the flow pattern evolves from slug flow to churn flow. U_{sg} and U_{sw}, in Fig. 11, represent gas superficial velocity and water superficial velocity, respectively.

B. Network information entropy

The concept of Shannon's entropy [40] is the central role of information theory sometimes referred to as measure of uncertainty. The entropy of a random variable is defined in terms of its probability distribution and can be shown to be a good measure of uncertainty. To calculate the information entropy I, Shannon also gave the equation as follows:

$$I = k_B \ln \Omega = -\sum_{j=1}^{N} k_B P(j) \ln P(j), \tag{19}$$

where Ω is the information; $P(j)=1/\Omega$; k_B is the Boltzmann constant.

According to the definition of Shannon's entropy, we define network information entropy for the FDCN and expect to investigate the nonlinear dynamics of gas-liquid flow through analyzing the network information entropy.

Definition 1: let $p(i)$ be the importance of node i:

$$p(i) = k_i / \sum_{j=1}^{N} k_j, \tag{20}$$

where N is the number of nodes contained in the network; k_i (k_j) is the degree of node i (j).

Definition 2: let E be the network information entropy:

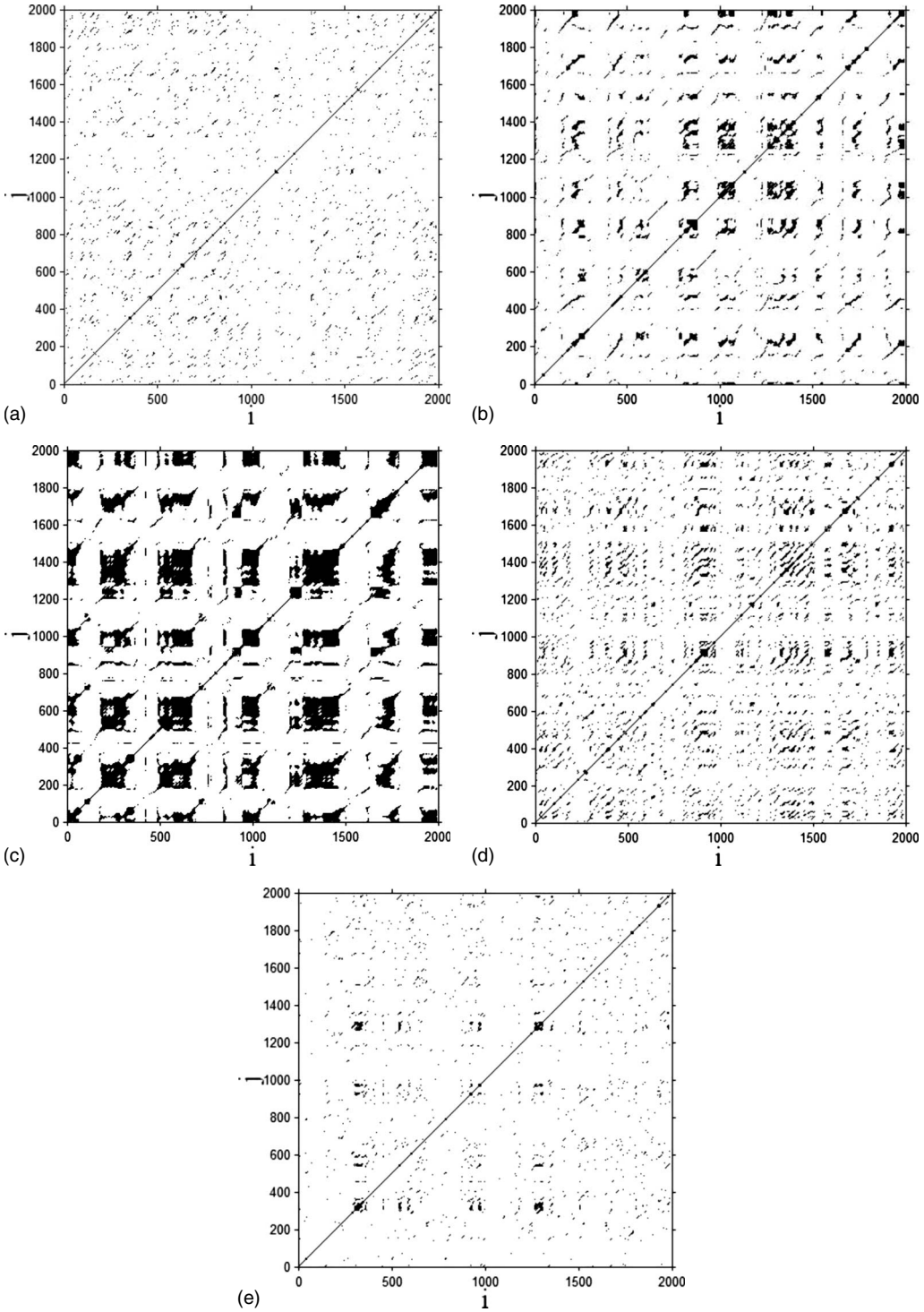

FIG. 10. Texture of recurrence plot of five flow patterns. (a) Bubble flow (Q_g=0.2 m^3/h, Q_w=2.0 m^3/h); (b) bubble-slug transitional flow (Q_g=1.0 m^3/h, Q_w=2.0 m^3/h); (c) slug flow (Q_g=4.1 m^3/h, Q_w=6.0 m^3/h); (d) slug-churn transitional flow (Q_g=25.0 m^3/h, Q_w=4.0 m^3/h); (e) churn flow (Q_g=139.0 m^3/h, Q_w=2.0 m^3/h).

$$E = -\sum_{i=1}^{N} k_B p(i) \ln p(i), \tag{21}$$

where N is the number of nodes contained in the network and k_B is the Boltzmann constant. In order to simplify the calculation, here we let k_B=1, that is:

$$E = -\sum_{i=1}^{N} p(i) \ln p(i). \tag{22}$$

In order to make the network information entropy not affected by the number of nodes contained in the network, we normalize E as follows:

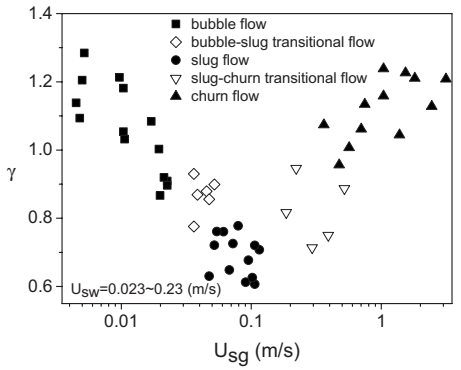

FIG. 11. The power-law exponent distribution in semilog scale of 50 FDCNs with the increase in gas superficial velocity.

$$E_N = \frac{E - E_{\min}}{E - E_{\max}} = \frac{-\sum_{i=1}^{N} p(i)\ln p(i) - \frac{\ln 4(N-1)}{2}}{-\sum_{i=1}^{N} p(i)\ln p(i) - \left(-\sum_{i=1}^{N} \frac{1}{N}\ln\frac{1}{N}\right)}. \tag{23}$$

We calculate the network information entropy from the 50 constructed FDCNs. Figure 12 shows the variations in network information entropy with the change in flow pattern. As can be seen, the network information entropy decreases as the flow pattern evolves from bubble flow to slug flow but increases as the flow pattern evolves from slug flow to churn flow.

C. Nonlinear dynamics of gas-liquid two-phase flow

Representing the conductance fluctuation signal through a corresponding FDCN, we can then explore the nonlinear dynamics of gas-liquid two-phase flow from network organization, which is quantified via a number of topological statistics. The previous study of our research team has indicated that the Lempel and Ziv complexity [41], and approximate entropy [42] are sensitive to the flow pattern transition in gas-liquid two-phase flow (for details, see reference [43]). Here we show, in Fig. 13, the variations in these two complexity measures with the change in flow pattern. From Figs. 11 and 12 as well as Fig. 13, we could see that there are good

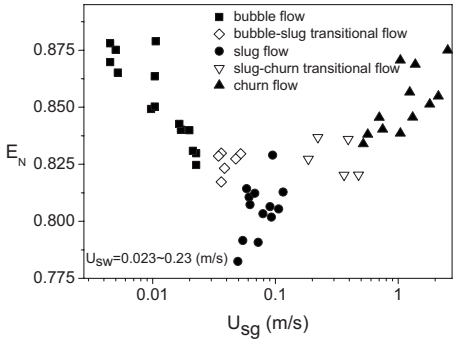

FIG. 12. The network information entropy distribution in semilog scale of 50 FDCNs with the increase in gas superficial velocity.

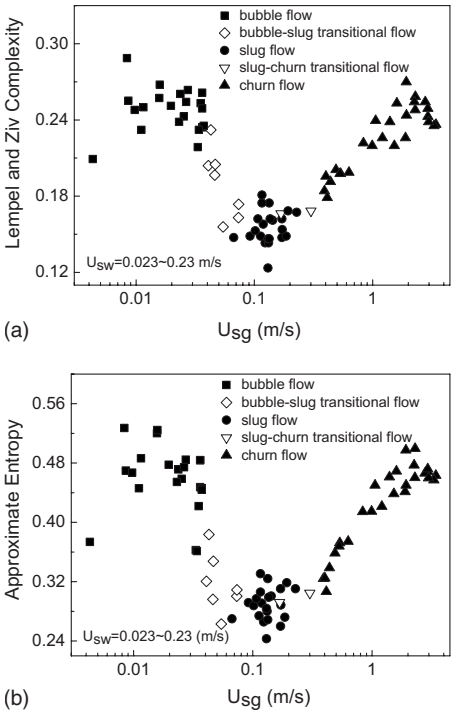

FIG. 13. The complexity measure distributions in semilog scale with the increase in gas superficial velocity. (a) Lempel and Ziv complexity (using four-symbol coarse graining); (b) approximate entropy.

corresponding relations between complexity measures and the FDCN topological statistics (i.e., power-law exponent and network information entropy). When the gas superficial velocity is low due to the stochastic motion of large number of small bubbles, the dynamics of bubble flow are very complex, corresponding to the large power-law exponent and network information entropy. In the transition from bubble flow to slug flow, the dynamics of this transitional flow becomes relatively simple, resulting in the decrease in the two network statistics. Owing to the periodic alternating movements between gas and liquid plugs, the dynamics of slug flow are very simple and that is why the two network statistics decrease as the flow pattern evolves from bubble flow to slug flow. When the gas superficial velocity is high, churn flow, which is composed of discrete gas phase and continuous liquid phase of high turbulent kinetic energy, gradually appears with the phenomenon of fluctuation. Because of the influence of the turbulence effect, the dynamics of churn flow becomes more complex than that of slug flow, corresponding to the increase in the two network statistics as the flow pattern evolves from slug flow to churn flow. Hence, the power-law exponent and network information entropy, which are sensitive to the flow pattern transition, can both characterize the nonlinear dynamics of gas-liquid two-phase flow.

VIII. COMPLEX NETWORK FROM TIME SERIES BASED ON PHASE SPACE RESCONSTRUCTION

In fact, the traditional nonlinear time-series analysis methods (chaotic attractor morphology, complexity measures, and

chaotic recurrence plot) cannot effectively reveal the complex fluid structure of gas-liquid two-phase flow. Although the network construction algorithm mentioned in Sec. VI can be applied to investigate the fluid dynamics of gas-liquid two-phase flow to a certain extent, it may have difficulties in getting enough information to study the fluid structure of two-phase flow. An important advantage of utilizing a phase-space reconstruction is that, if the embedding is chosen appropriately, the topological distribution of the set of vector points in phase space will accurately reflect the underlying dynamics of the original system. Therefore, the network inferred from that phase-space reconstruction can be related directly back to the evolution operator of the underlying dynamical system.

In this section, we not only propose a general method for constructing complex network from a time series based on phase-space reconstruction but also associate different aspects of the dynamics of the time series with the topological indices of the network. Moreover, we demonstrate how such statistics can be used to distinguish different dynamical regimes.

We start from the phase-space reconstruction. Takens' embedding theorem [44], which is very often invoked as the motivation for applying a time delay embedding to reconstruct phase space from a time series, can be described as following for arbitrary time series $z(it)$, $i=1,2\ldots,M$ (t is sampling interval, M is the sample size); if the embedding delay time is selected as τ, and the embedding dimension as m, the vector point in phase space can be represented as follow:

$$\begin{aligned}\overrightarrow{X_k} &= \{x_k(1), x_k(2), \ldots, x_k(m)\} \\ &= \{z(kt), z(kt+\tau), \ldots, z[kt+(m-1)\tau]\}, \end{aligned} \tag{24}$$

where $k=1,2,\ldots,N$, $N=M-(m-1)^*\tau/t$ denotes the total vector points of the reconstructed phase space. C-C method [33] is the frequent method that can be used for determining the delay time τ and embedding dimension m. Through studying four algorithms that can be used for selecting τ, i.e., mutual information-I [45], mutual information-II [46], autocorrelation function method, and C-C method, our research team has in Ref. [47] indicated that C-C method shows good antinoise ability. Hence, we in this section using C-C method reconstruct phase space from time series.

After reconstructing phase space from a given time series, denoted as $\{z(1),z(2),\ldots,z(M)\}$, we proceed to construct complex network by considering each vector point in reconstructed phase space as a basic node and using the phase-space distance to determine network connection. The phase-space distance between vector points $\overrightarrow{X_i}$ and $\overrightarrow{X_j}$, in this study, is defined as

$$d_{ij} = \sum_{n=1}^{m} \|X_i(n) - X_j(n)\|, \tag{25}$$

where $X_i(n)=z[i+(n-1)\tau]$ and $X_j(n)=z[j+(n-1)\tau]$ is the nth element of $\overrightarrow{X_i}$ and $\overrightarrow{X_j}$, and m and τ is the embedding dimension and delay time, respectively. Choosing a critical threshold r_c, the distance matrix $\boldsymbol{D}=(d_{ij})$ can be converted into adjacent matrix $\boldsymbol{A}=(a_{ij})$, the rules of which read: $a_{ij}=1$ if $d_{ij}\leq r_c$ and $a_{ij}=0$ if $d_{ij}>r_c$. The topological structure of the network can be described with the adjacent matrix $\boldsymbol{A}$, and the conditions $a_{ij}=1$ and $a_{ij}=0$ correspond to connection and disconnection, respectively.

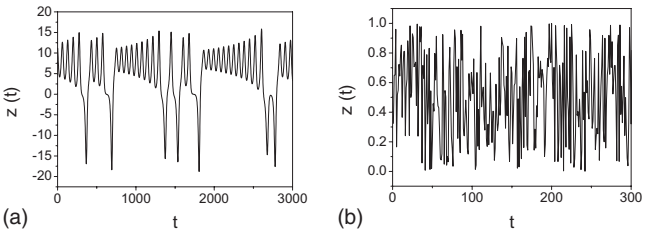

FIG. 14. Two different time series that are used to construct complex networks. (a) Chaotic time series from Lorenz system; (b) white-noise time series.

An appropriate threshold therefore should be chosen to fully preserve the main property of the network but not to be too large that it may obscure or conceal the local property by overconnecting the nodes. We employ the network density [29] to study the threshold, which is defined as the number of edges divided by the largest number of edges possible. In order to show how to select a suitable threshold, a chaotic time series from Lorenz system [see Fig. 14(a)] is studied by this method, and Fig. 15 shows the density of the constructed network versus the threshold r. As can be seen in Fig. 15(b), the increase in degree reaches the maximum rate at about $r_c=7.6$, where we set the critical threshold. We explain here why we set the threshold r at this critical point. It can be imagined that the degree increases more rapidly as the threshold changes within the cluster radius due to the adjacency of the nodes inside. For a network from a chaotic system that has many clusters differing in sizes, it can be further imagined that the edge increase will arrive at the maximum rate as the threshold approaches the critical point r_c, i.e., the "mean radius" of all the clusters. The network obtained at r_c will maintain the clustering property, and thresholds beyond this value will result in a much slower edge increase, causing redundant connections among nodes. Consequently we choose r_c to derive the network. Furthermore, it should be noted that the size of the network (the length of the time series) will influence r_c.

Before further analysis, we here give an intuitive description of the loop layout in phase space for chaotic systems in terms of the unstable periodic orbits (UPOs). Unstable periodic orbits embedded in the chaotic attractor are fundamental

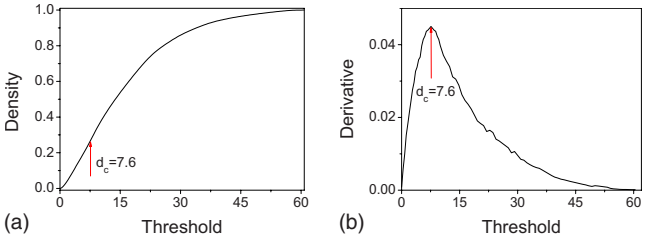

FIG. 15. (Color online) Complex network from the Lorenz system with 600 nodes. (a) Density versus threshold; (b) Derivative of density versus threshold, with $r_c=7.6$.

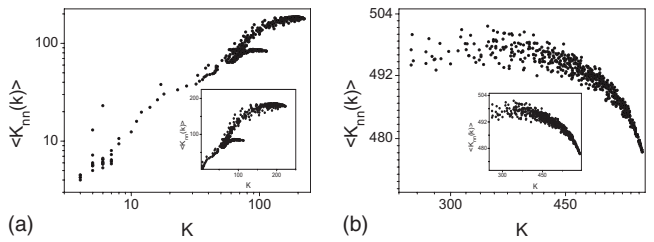

FIG. 16. The log-log plots of the nearest-neighbor average connectivity of nodes with respect to connectivity (insets: the regular plots) of the networks containing 600 nodes from (a) Lorenz system with $r_c=7.6$ and (b) white-noise time series with $r_c=0.8$.

to the understanding of the chaotic dynamics [48,49]. For a chaotic attractor, its trajectory will typically switch or hop among different UPOs. Specifically, the trajectory will approach an unstable periodic orbit along its stable manifold. This approach can last for several loops during which the orbit remains close to the UPO. Eventually, the orbit is ejected along the unstable manifold and proceeds until it is captured by the stable manifold of another UPO. A UPO of order n contains n loops lying in different locations in phase space. Each loop that belongs to a certain UPO-n has many other loops in its vicinity due to the attraction of the stable manifold associated with the UPO-n. It then becomes a center of a cluster and the density of the neighbors is related to its stability decided by the vector field along its trajectory. Since the stability of each center loop may vary, there are sparse as well as dense regions in the structure of constructed complex network. Due to the fact that the loops in phase space are spatially clustered around the UPOs and we are using phase space to determine the network connection, there are multiple clusters in the complex network generated from chaotic time series.

We now demonstrate how to discriminate different dynamical regimes of the time series through investigation of the degree correlations and Pearson coefficient of two distinct complex networks from the chaotic time series (Lorenz system) and white-noise time series (details of the two different time series can be seen in Fig. 14). An important way of capturing the degree correlations is to examine the average degree of the nearest neighbors of nodes with degree k [50], which is defined as

$$k_{nn}(k) = \sum_{k'} k' P(k'|k), \tag{26}$$

where $P(k'|k)$ denotes the conditional probability that an edge of degree k connects a node with degree k'. If there are no degree correlations, Eq. (26) gives $k_{nn}(k)=\langle k^2\rangle/\langle k\rangle$, i.e., $k_{nn}(k)$ is independent of k. Correlated networks are classified as assortative mixing if $k_{nn}(k)$ is an increasing function of k, whereas they are referred to as disassortative mixing when $k_{nn}(k)$ is a decreasing function of k. In other words, in assortative networks the nodes tend to connect to their connectivity peers while in disassortative networks nodes with low degree are more likely connected with highly connected ones. As can be seen in Fig. 16, $k_{nn}(k)$ increases with k for chaotic Lorenz system while it decreases with k for noisy time series. In order to quantify such a correlation, we also calculate the Pearson coefficient [51] which is defined as follows. Let $e_{kl}(=e_{lk})$ be the joint probability distribution for an edge to be with a node with connectivity k at one end and a node with connectivity l at the other. Its marginal, $q_k=\Sigma_l e_{kl}$, obeys the normalization condition, $\Sigma_k q_k=1$. Then, the Pearson correlation coefficient is given by

$$r = \frac{1}{\sigma_q^2}\sum_{k,l} kl(e_{kl} - q_k q_l), \tag{27}$$

where $\sigma_q^2=\Sigma_k k^2 q_k-(\Sigma_k k q_k)^2$ is the variance of q_k $r\in[-1,1]$, and r is positive (negative) for assortative (disassortative) mixing. The Pearson coefficient of the network containing 600 nodes from chaotic Lorenz system and noisy time series is 0.2297 and −0.0037, respectively. Consistently with the one obtained from the analysis of the nearest-neighbor average connectivity, the Pearson correlation coefficient is positive, confirming that the network from chaotic time series has assortative mixing. On the other hand, the network from noisy time series is of disassortative mixing. We can explain why the network corresponding to chaotic time series possesses the property of assortative mixing in terms of UPOs. For a complex network generated from chaotic time series, there are multiple clusters and most nodes connected to each other within the same cluster have a roughly similar number of connected neighbors or degrees (except for a few on the margin of the cluster). The common degree shared by the nodes from one cluster may differ from that of another because of the different stability of the center loop of UPOs. This has led to the fact that nodes with similar degrees are interconnected to each other, i.e., assortative mixing, because they belong to the same cluster.

In summary, we in this section have proposed an effective method for constructing complex network from a time series, and it is worth pointing out that this method can be used for analyzing time series from any kind of complex system. Through investigating the complex networks generated from two different complex dynamic systems, we find that the constructed network inherits main properties of the time series in its structure. Furthermore, by exploring the network topology statistics, we have demonstrated that the degree correlations and Pearson coefficient can fundamentally reflect the clustering property of the nodes induced by the UPOs. Construction of networks from time series is a common problem in diverse research. The proposed strategy may be a reasonable solution to this problem.

IX. FLUID STRUCTURE OF GAS-LIQUID FLOW IN FSCN

We construct fluid structure complex network (FSCN) of 2000 nodes using the method mentioned in Sec. VIII and make a further investigation on their assortative mixing property. The structure of FSCNs with 200 nodes generated from three typical flow patterns are shown in Fig. 17.

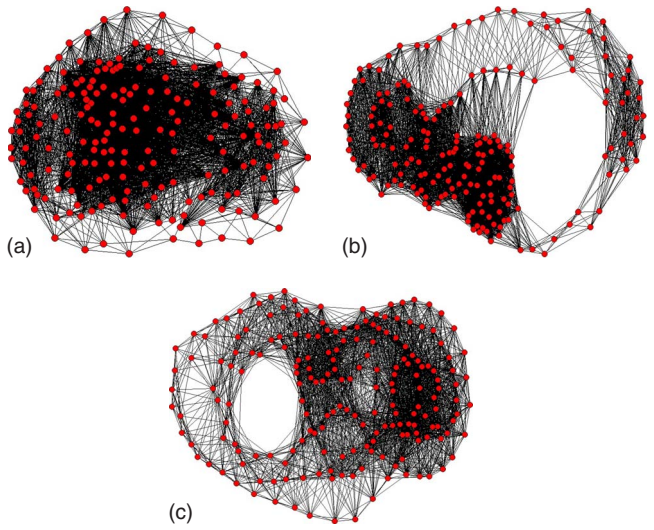

FIG. 17. (Color online) The structure of FSCN containing 200 nodes from (a) bubble flow (Q_g=0.2 m^3/h, Q_w=2.0 m^3/h) with r_c=0.012, (b) slug flow (Q_g=4.1 m^3/h, Q_w=6.0 m^3/h) with r_c=0.16, and (c) churn flow (Q_g=139.0 m^3/h, Q_w=2.0 m^3/h) with r_c=0.11.

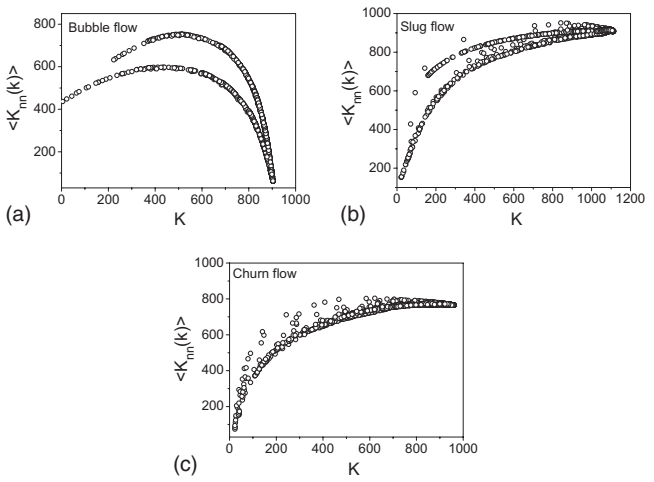

FIG. 18. The regular plots of the nearest-neighbor average connectivity of nodes with respect to connectivity of the networks containing 2000 nodes from (a) bubble flow (Q_g=0.2 m^3/h, Q_w=2.0 m^3/h) with r_c=0.031, (b) slug flow (Q_g=4.1 m^3/h, Q_w=6.0 m^3/h) with r_c=0.35, and (c) churn flow (Q_g=139.0 m^3/h, Q_w=2.0 m^3/h) with r_c=0.26.

We now demonstrate how the statistic of FSCN can be used to reveal the fluid structure of gas-liquid two-phase flow. In the bubble flow, the gas phase is approximately uniformly distributed in the form of discrete small bubbles in a continuum of liquid phase, and no obvious bubble coalescence can be observed. While in the slug flow, due to the bubble coalescence, many large bubbles which have a diameter almost equal to the pipe diameter appear. Bubble coalescence, which has an important impact on the fluid structure of gas-liquid two-phase flow, can be reflected by many UPOs in the reconstructed phase space. For a FSCN from slug flow, there are multiple clusters which are caused by the bubble coalescence, and most nodes connected to each other within the same cluster have a roughly similar number of connected neighbors or degrees. The common degree shared by the nodes from one cluster may differ from that of another because of the different stability of the center loop of UPOs. This has led to the fact that the FSCN from slug flow possesses the property of strong assortative mixing [for details, see Fig. 18(b)], while no assortative mixing can be found in the FSCN from bubble flow [see Fig. 18(a)]. Churn flow can be interpreted as an irregular, chaotic, and disordered slug flow. Since bubble coalescence and bubble collapse both exist in the fluid structure of churn flow, the FSCN from churn flow also possesses the property of assortative mixing. But compared with the FSCN from slug flow, the FSCN from churn flow shows weak assortative mixing, which may be caused by the bubble collapse [for details, see Fig. 18(c)].

Therefore, we have associated the fluid structure of gas-liquid two-phase flow with the topological indices of FSCN, and indicate that the assortative mixing property of FSCN can effectively reveal the gas-liquid fluid structure to some extent.

X. CONCLUSIONS

In summary, we have introduced complex network theory to the study of gas-liquid two-phase flow. Using a unique method based on time-delay embedding and modularity, we construct FPCN from conductance fluctuating signals. Then we put forward a unique flow pattern identification method of gas-liquid two-phase flow by combining the community structure of FPCN.

In order to study the nonlinear dynamics of gas-liquid two-phase flow, 50 FDCNs under different flow conditions are constructed, and the nonlinear dynamics can then be studied by investigating the statistical characteristics of those networks. Moreover, using the method of chaotic recurrence plot, we have discussed the physical implications of the degree distribution of FDCNs. Based on the investigation of the statistical characteristics of FDCNs, we confirm that the power-law exponent and network information entropy, which are sensitive to the flow pattern transition, can both characterize the nonlinear dynamics of gas-liquid two-phase flow.

Since the FDCN as well as the traditional nonlinear time-series analysis methods [PSD, Wigner-Ville Distribution (WVD)], chaotic attractor morphology, complexity measures, and chaotic recurrence plot) cannot effectively reveal the complex fluid structure of gas-liquid two-phase flow, we propose a general method, which can be used for analyzing time series from any kind of complex system, to study the fluid structure of gas-liquid two-phase flow. We construct FSCN using this method and demonstrate that the distinction in topological structure of FSCN can really reflect the bubble coalescence and bubble collapse in gas-liquid fluid structure.

The last decade has witnessed the birth of a new movement of interest and research in the study of complex networks, and the massive and comparative analysis of networks from different fields have produced a series of unexpected and dramatic results. With the study presented in this paper, a natural bridge between complex networks and two-phase flow has now been built. Further research on the self-organizing and self-evolution in these networks will help us establish a flow-evolution network model to explore the complex mechanism in two-phase flow.

ACKNOWLEDGMENTS

This work has been supported by National Natural Science Foundation of China (Grants No. 50674070 and No. 60374041), and National High Technology Research and Development Program of China (Grant No. 2007AA06Z231).

[1] S. Z. Rouhani and M. S. Sohal, Prog. Nucl. Energy **11**, 219 (1983).
[2] R. K. Das and S. Pattanayak, Meas. Sci. Technol. **4**, 1457 (1993).
[3] M. G. Hubbard and A. E. Dukler, *Proceedings of the 1966 Heat Transfer and Fluid Mechanics Institute* (Stanford University Press, Stanford, CA, 1966).
[4] O. C. Jones, Jr. and N. Zuber, Int. J. Multiphase Flow **2**, 273 (1975).
[5] M. A. Vince and R. T. Lahey, Jr., Int. J. Multiphase Flow **8**, 93 (1982).
[6] Z. Y. Zhang and L. Shi, J. Appl. Phys. **85**, 7544 (1999).
[7] C. S. Daw, W. F. Lawkins, D. J. Downing, and N. E. Clapp, Jr., Phys. Rev. A **41**, 1179 (1990).
[8] W. F. Lawkins, C. S. Daw, D. J. Downing, and N. E. Clapp, Jr., Phys. Rev. E **47**, 2520 (1993).
[9] C. S. Daw, C. E. A. Finney, M. Vasudevan, N. A. vanGoor, K. Nguyen, D. D. Bruns, E. J. Kostelich, C. Grebogi, E. Ott, and J. A. Yorke, Phys. Rev. Lett. **75**, 2308 (1995).
[10] Y. Mi, M. Ishii, and L. H. Tsoukalas, Nucl. Eng. Des. **204**, 87 (2001).
[11] W. Warsito and L. S. Fan, Meas. Sci. Technol. **12**, 2198 (2001).
[12] H. Yan, Y. H. Liu, and C. T. Liu, Meas. Sci. Technol. **15**, 432 (2004).
[13] N. Xiao and N. D. Jin, Acta Phys. Sin. **56**, 5149 (2007).
[14] D. J. Watts and S. H. Strogatz, Nature (London) **393**, 440 (1998).
[15] A.-L. Barabási and R. Albert, Science **286**, 509 (1999).
[16] R. Albert, H. Jeong, and A.-L. Barabási, Nature (London) **401**, 130 (1999).
[17] H. Jeong, B. Tombor, R. Albert, Z. N. Oltvai, and A.-L. Barabási, Nature (London) **407**, 651 (2000).
[18] H. Jeong, S. Mason, A.-L. Barabási, and Z. N. Oltvai, Nature (London) **411**, 41 (2001).
[19] X. G. Li, Z. Y. Gao, K. P. Li, and X. M. Zhao, Phys. Rev. E **76**, 016110 (2007).
[20] F. Liljeros, C. R. Edling, L. A. N. Amaral, H. E. Stanley, and Y. Aberg, Nature (London) **411**, 907 (2001).
[21] S. Abe and N. Suzuki, Phys. Rev. E **74**, 026113 (2006).
[22] S. M. Cai, Z. H. Jiang, T. Zhou, P. L. Zhou, H. J. Yang, and B. H. Wang, Phys. Rev. E **76**, 061903 (2007).
[23] C. P. Zhu, S. J. Xiong, Y. J. Tian, N. Li, and K. S. Jiang, Phys. Rev. Lett. **92**, 218702 (2004).
[24] W. X. Wang, B. H. Wang, C. Y. Yin, Y. B. Xie, and T. Zhou, Phys. Rev. E **73**, 026111 (2006).
[25] S. Çalışkan, M. A. Novotny, and J. I. Cerdá, J. Appl. Phys. **102**, 013707 (2007).
[26] F. Luo, J. Zhong, Y. Yang, and J. Zhou, Phys. Rev. E **73**, 031924 (2006).
[27] J. Zhang and M. Small, Phys. Rev. Lett. **96**, 238701 (2006).
[28] Y. Yang and H. J. Yang, Physica A **387**, 1381 (2008).
[29] J. Zhang, J. F. Sun, X. D. Luo, K. Zhang, T. Nakamura, and M. Small, Physica D **237**, 2856 (2008).
[30] G. F. Hewitt, *Measurement of Two-Phase Flow Parameters* (Academic Press, London, 1980).
[31] N. D. Jin, Z. Xin, J. Wang, Z. Y. Wang, X. H. Jia, and C. P. Chen, Meas. Sci. Technol. **19**, 045403 (2008).
[32] N. H. Packard, J. P. Crutehfield, and J. D. Farmer, Phys. Rev. Lett. **45**, 712 (1980).
[33] H. S. Kim, R. Eykholt, and J. D. Salas, Physica D **127**, 48 (1999).
[34] M. E. J. Newman, Phys. Rev. E **69**, 066133 (2004).
[35] T. D. Darwich, H. Toral, and J. S. Archer, SPE Prod. Eng. **8**, 265 (1991).
[36] H. Makhoul, Proc. IEEE **63**, 561 (1975).
[37] A. Capocci, V. D. P. Servedio, G. Caldarelli, and F. Colaiori, Physica A **352**, 669 (2005).
[38] K. Rho, H. Jeong, and B. Kahng, Physica A **364**, 557 (2006).
[39] J. P. Eckmann, S. O. Kamphorst, and D. Ruelle, Europhys. Lett. **4**, 973 (1987).
[40] C. E. Shannon, Bell Syst. Tech. J. **27**, 379 (1948).
[41] A. Lempel and J. Ziv, IEEE Trans. Inf. Theory **22**, 75 (1976).
[42] S. M. Pincus, Proc. Natl. Acad. Sci. U.S.A. **88**, 2297 (1991).
[43] N. D. Jin, F. Dong, and S. Zhao, Acta Phys. Sin. **56**, 0720 (2007).
[44] F. Takens, Lect. Notes Math. **898**, 366 (1981).
[45] A. M. Fraser and H. L. Swinney, Phys. Rev. A **33**, 1134 (1986).
[46] W. Liebert and H. G. Schuster, Phys. Lett. A **142**, 107 (1989).
[47] N. D. Jin, G. B. Zheng, and L. Y. Hu, Chin. J. Geophys. **49**, 1552 (2006).
[48] D. Auerbach, P. Cvitanovic, J.-P. Eckmann, G. Gunaratne, and I. Procaccia, Phys. Rev. Lett. **58**, 2387 (1987).
[49] B. Hunt and E. Ott, Phys. Rev. Lett. **76**, 2254 (1996).
[50] R. Pastor-Satorras, A. Vázquez, and A. Vespignani, Phys. Rev. Lett. **87**, 258701 (2001).
[51] M. E. J. Newman, Phys. Rev. Lett. **89**, 208701 (2002).